Evidence for spin injection in a single metallic nanoparticle: A step towards nanospintronics

A. Bernand-Mantel, P. Seneor,[a] N. Lidgi, M. Muñoz,[b] V. Cros, S. Fusil, K. Bouzehouane, C. Deranlot, A. Vaures, F. Petroff, and A. Fert
Unité Mixte de Physique CNRS/Thales and Université Paris-Sud 11, 91767 Palaiseau, France

(Received 7 November 2005; accepted 22 June 2006; published online 7 August 2006)

We have fabricated nanometer-sized magnetic tunnel junctions using a conductive tip nanoindentation technique in order to study the transport properties of a single metallic nanoparticle. Coulomb blockade effects show clear evidence for single-electron tunneling through a single 2.5 nm Au cluster. The observed magnetoresistance is the signature of spin conservation during the transport process through a *nonmagnetic* cluster. © *2006 American Institute of Physics*.
[DOI: 10.1063/1.2236293]

Spintronics debuted with the discovery of giant magnetoresistance[1] effect in magnetic multilayers in which a single dimension was reduced to the nanometer range. This field was then extended to structures with two reduced dimensions like nanowires[2] and nanopillars[3,4] or nanotubes.[5] Today, a challenge for spintronics is the study of spin transport properties in structures based on zero-dimensional elements in which the three dimensions have been reduced. In particular, we have in mind systems in which the reduction of the size leads to both Coulomb blockade and spin accumulation effects.[6–8] Transport studies on systems including mesoscopic islands[9–11] or granular films[12–14] have paved the way to understanding the effect of confinement on charge and spin transport properties in metallic nano-objects. However, so far, very few techniques allow to contact a single isolated nanometer sized object[15–17] to study the effect of confinement on spin transport.

In this letter we present the experimental achievement of a technique allowing us to inject and detect spins in a single isolated nanometer-sized cluster. We then obtain information on both spin and single-electron transport in the nanoparticle. In this technique, a ferromagnetic nanocontact with a cross section of $\sim 5-10$ nm in diameter is created on a bilayer associating a cobalt layer and an ultrathin alumina layer in which a two-dimensional (2D) assembly of gold nanoparticles is embedded (see Fig. 1 for a sketch). As we will show, this structure allows the tunneling of electrons into and out of a single Au nanoparticle.

The whole structure is elaborated in a sputtering system (base pressure 5×10^{-8} mbar) with Ar gas at a dynamic pressure of 2.5×10^{-3} mbar. The deposition of a bilayer of Co(15 nm)/Al(0.6 nm) is followed by the oxidization of the Al layer in pure O_2 (50 mbar for 10 min) to form the first tunnel barrier. Then, an ultrathin layer of Au (0.2 nm nominal thickness) is deposited on top of the bilayer. The three-dimensional growth (see Ref. 18) of the sputtered gold on top of alumina produces a self-formed nanoparticles layer. A plane view transmission electron microscopy (TEM) picture of the Au nanoparticles 2D self-assembly is shown in Fig. 2. The size distribution of the Au nanoparticles is characterized by a 2-nm-diam mean value and a 0.5 nm standard deviation with a density of $1.7\cdot10^{12}$ cm^{-2}. Finally, the Au clusters are capped by another Al layer (0.6 nm) subsequently oxidized in pure O_2 with the same process used to form the first tunnel barrier. This creates a Co/Al_2O_3 bilayer with Au nanoclusters embedded in the thin alumina layer.

To define an electrical contact on a single cluster we use a four step process combining atomic force microscopy (AFM) and optical lithographic techniques (for further technical details see Ref. 19). For the first step, a photoresist layer of 35 nm is spin coated over the whole $Co/Al_2O_3/Au/Al_2O_3$ structure. Then, contact zones are defined using a second photoresist layer and a standard UV lithography process. During the second step a conductive boron doped diamond AFM tip is used to nanoindent the thin resist. The conductance between the conductive sample and the AFM tip is monitored in real time. In the late stage of the nanoindentation a tunneling current is established between the tip and the sample. The exponential thickness dependence allows to precisely control the end of the indentation process. The tip is then retracted and the sample is left with a nanometer scale hole on the surface. After this nanoindentation process, the holes can be inspected by tapping mode AFM using ultrasharp tips. In Fig. 1, we show the cross section of a typical hole after enlargement by a 30 s O_2 plasma etch. On the cross section one can see that the contact area section is in the 10 nm range. The samples presented in this letter use a shorter enlarging plasma etch of 20 s giving hole sections below the 10 nm range. However, due to a tip nominal radius of 5 nm, holes having a contact cross section below 10 nm cannot be properly imaged.[19] From the nanoparticles density of $1.7\cdot10^{12}$ cm^{-2} and assuming a disk shape area for the contact surface, there is an average of 0.3–1.2 nanoparticles per nanocontact hole for holes diameter in the 5–10 nm range. The next step is the filling of the hole by a sputtered Co 15 nm/Au 50 nm counter electrode, just after a short O_2 plasma. Finally, we use standard optical lithography and ion beam etching techniques to define the top electrode. This allows us to obtain a *single* cluster per nanocontact with a high expectation value.

The patterned samples were measured in a variable temperature cryostat from 4.2 to 300 K. In Fig. 3, one can see the $dI/dV(V)$ curves of a nanopatterned sample at different

[a]Author to whom correspondence should be addressed; electronic mail: pierre.seneor@thalesgroup.com
[b]Now at Laboratorio de Física de Sistemas Pequeños y Nanotecnología, Consejo Superior de Investigaciones Científicas, Serrano 144, 28006 Madrid, Spain.

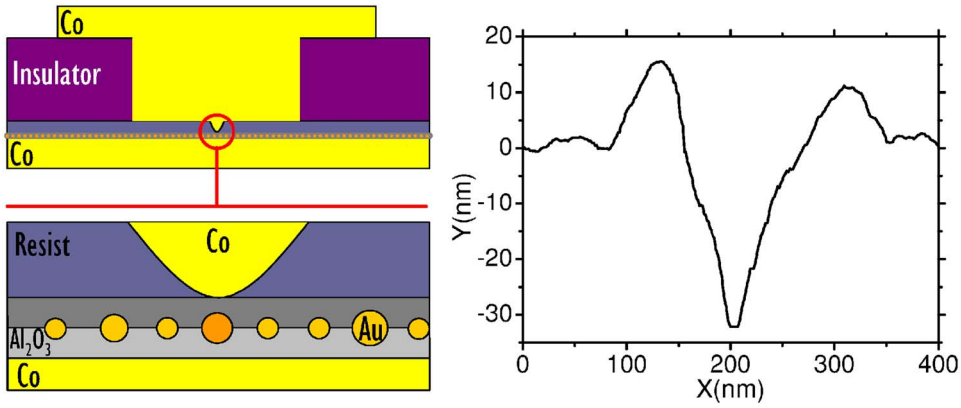

FIG. 1. (Color online) Left: Schematic cross section of the whole patterned structure showing the top/bottom Co electrodes and the 2D assembly of nanoparticles embedded in a thin alumina layer. The circle represents the zone zoomed in the bottom drawing. Right: Cross section of an AFM tapping mode scan of a nanoindent before filling with the Co top electrode. The effective nanocontact cross section is less than 10 nm.

temperatures. Above 190 K the conductance curve presents tunnel-like features without any evidence of Coulomb blockade. At 120 K, shoulders characteristic of Coulomb blockade start to appear in the conductance curve and get more pronounced as temperature is lowered. Considering a single nanoparticle, for Coulomb blockade to be observed at 120 K, the charging energy E_C of the nanoparticle has to be greater than about $kT_{120\ \mathrm{K}}$ which suggests that the charging energy is at least $\simeq$10 meV. Below 60 K an asymmetry in the shoulder position, typical of the presence of a nonzero Q_0 background offset charge,[20] can be observed in the conductance curves. At 4.2 K, the Coulomb blockade peaks are clearly visible, with an equal spacing of $V_s \simeq 140$ mV between peaks. As the highest capacitance governs the peak spacing, we extract $C_{\max}=1.14$ aF from V_s through $C_{\max}=e/V_s$. This parameter is used as an input for the single nanoparticle Monte Carlo simulation (MOSES)[21] which faithfully reproduces the peaks of the 4.2 K conductance curve in Fig. 3. In this simulation, the structure is modelized as two tunnel junctions in series. Using $C_2=C_{\max}=1.14$ aF and $T=4.2$ K, the best fitting parameters for the two tunnel junctions are $C_1=0.4$ aF, $R_2=3R_1$ and a background charge of $Q_0/e=0.4$. A V^2 term is added to the simulated curve to take into account the quadratic variation of the tunnel conductance versus voltage.[22] The charging energy E_C of the nanoparticle can then be calculated assuming the nanoparticle total capacitance is $C_T=C_1+C_2$. One finds $E_C=e^2/2C_T \simeq 50$ meV which is in agreement with the fading of the Coulomb blockade features above 120 K. Using electrostatic simulations and the capacitances extracted from the fit, we can determine the nanoparticle diameter to be $\simeq$2.5 nm in excellent agreement with the average size determined by TEM.

In Fig. 4, $I(V)$ and dI/dV curves at 4.2 K of the same sample are shown after a sweep at higher voltage. A change in the background charge has occurred. The curves are almost symmetric in voltage bias which reflects the very low offset of the new background charge. A simulation curve using the same set of parameters as before, except for a smaller charge offset of $Q_0/e=0.07$, is also shown on the figure. A clear evidence that we observe single electron tunneling through a single isolated nanoparticle is that the same set of junctions parameters is used to obtain an excellent fit of our data with two different background charges. In the blockade region, we note the presence of a very low cotunneling current[23] not taken into account by the simulation.

We now focus on spin dependent transport in the sample. We measured tunnel magnetoresistance (TMR) with a clear definition of the parallel and antiparallel states of the magnetizations (see Fig. 5). Indeed, due to shape anisotropy, the top "cone" and the bottom plane magnetic electrodes

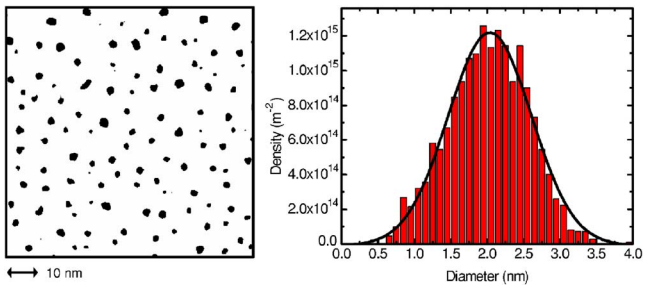

FIG. 2. (Color online) Left: Binarized plane view of self-assembled Au nanoparticles observed by TEM. See Ref. 18 for further information on the binarization process. Right: Size distribution of the same self-assembly. Fitting Gaussian (bold line), parameters are 2 nm mean diameter and 0.54 nm standard deviation.

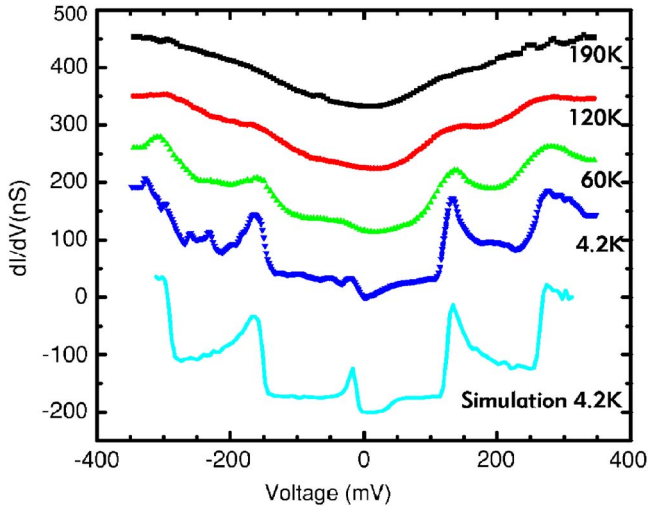

FIG. 3. (Color online) Differential conductance curves at, 190, 120, 60, and 4.2 K for a $Co/Al_2O_3/Au$ 0.2 nm nominal/$Al_2O_3/Co/Au$ nanocontact. Monte Carlo simulation (plain line) at 4.2 K and with a background charge offset $Q_0/e=0.4$. The other simulation parameters are $C_1=0.4$ aF, $C_2=1.14$ aF, $R_2=3R_1$.

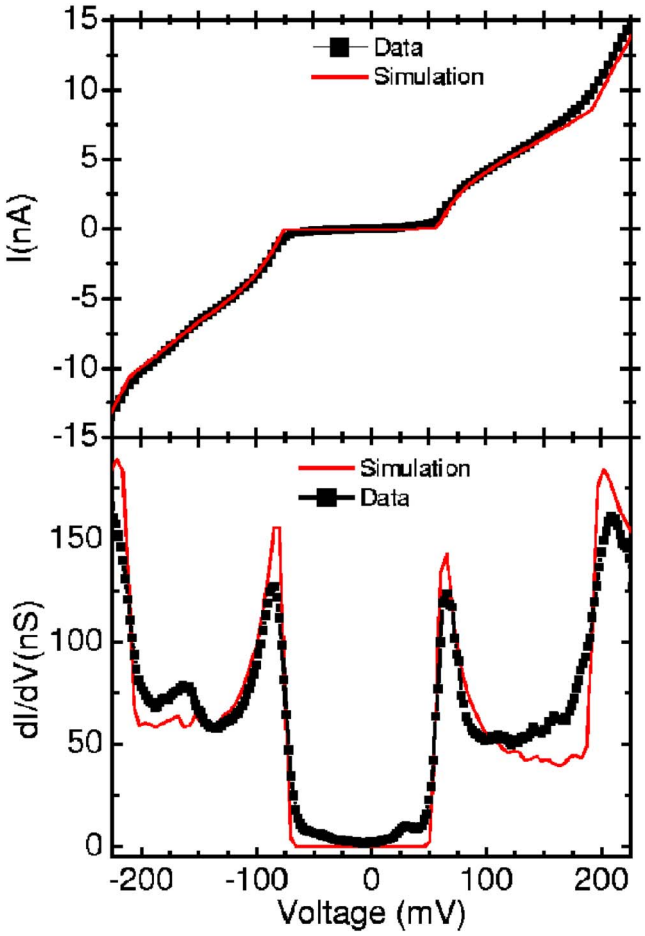

FIG. 4. (Color online) Top: $I(V)$ curve(■) measured at 4.2 K for the sample shown in Fig. 3 after a change in the background charge. The line is a simulation using the parameters given in the Fig. 3 caption but with $Q_0=0.07e$. Bottom: $dI/dV(V)$ curve (■) obtained from the derivative of the above $I(V)$ curve. The line represents the differentiation of the simulation.

have distinct coercive fields. TMR is observed in both cotunneling and sequential regime through the cluster. The occurrence of TMR is a direct proof of spin dependent transport in the nanostructure, which indicates spin injection from one electrode into the cluster and spin detection by the second electrode. As the cluster is nonmagnetic, the observation of TMR means that spin information is conserved in this transport process. Negative TMR effect has been predicted from the interaction of spin accumulation and Coulomb effects (namely magneto-Coulomb effects) on the nonmagnetic nanoparticle as discussed in Refs. 24 and 25 and has already been observed in magnetic granular films.[12,13] Moreover, we can rule out the existence of a shunting spin dependent transport path (other than through the cluster) leading to the observed TMR: direct tunneling between the two Co electrodes would lead to positive TMR at low bias and is furthermore exponentially suppressed by the double alumina barrier.

In summary, we have developed an original process to investigate the spin transport properties of a single nanoparticle and provided evidence for its successful realization. Our approach paves the way for a more in-depth study of magneto-Coulomb phenomena in nanosized clusters.

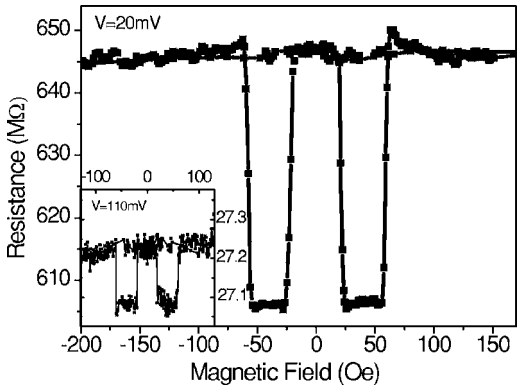

FIG. 5. Resistance vs magnetic field obtained at 20 mV and 4 K for the sample of Figs. 3 and 4. Inset: same sample at 110 mV.

The authors acknowledge the support of the EU through the Nanotemplates project (NMP-CT-2004-505955). They thank K. Reatur for fruitful discussions.

[1] M. N. Baibich, J. M. Broto, A. Fert, F. Nguyen van Dau, F. Petroff, P. Etienne, G. Creuzet, A. Friedrich, and J. Chazelas, Phys. Rev. Lett. **61**, 2472 (1988).
[2] L. Piraux, J. George, J. Despres, C. Leroy, E. Ferain, R. Legras, K. Ounadjela, and A. Fert, Appl. Phys. Lett. **55**, 2484 (1994).
[3] J. A. Katine, F. J. Albert, R. A. Buhrman, E. B. Myers, and D. C. Ralph, Phys. Rev. Lett. **84**, 3149 (2000).
[4] J. Grolier, V. Cros, A. Hamzic, J.-M. George, H. Jaffres, A. Fert, G. Faini, J. B. Youssef, and H. LeGall, Appl. Phys. Lett. **78**, 3663 (2001).
[5] K. Tsukagoshi, B. W. Alphenaar, and H. Ago, Nature (London) **401**, 572 (1999).
[6] J. Barnas and A. Fert, Phys. Rev. Lett. **80**, 1058 (1998).
[7] H. Imamura, S. Takahashi, and S. Maekawa, Phys. Rev. B **59**, 6017 (1999).
[8] A. Brataas, Y. V. Nazarov, and J. Inoue, Phys. Rev. B **59**, 93 (1999).
[9] M. Zaffalon and B. J. van Wees, Phys. Rev. B **71**, 125401 (2005).
[10] K. Ono, H. Shimada, and Y. Ootuka, J. Phys. Soc. Jpn. **66**, 1261 (1997).
[11] C. D. Chen, W. Kuo, D. S. Chung, J. H. Shyu, and C. S. Wu, Phys. Rev. Lett. **88**, 047004 (2002).
[12] S. Mitani, S. Takahashi, K. Takanashi, K. Yakushiji, S. Maekawa, and H. Fujimori, Phys. Rev. Lett. **81**, 2799 (1998).
[13] K. Yakushiji, F. Ernult, H. Imamura, K. Yamane, S. Mitani, K. Takanashi, S. Takahashi, S. Maekawa, and H. Fujimori, Nat. Mater. **4**, 57 (2005).
[14] L. F. Schelp, A. Fert, F. Fettar, P. Holody, S. Lee, J. L. Maurice, F. Petroff, and A. Vaures, Phys. Rev. B **56**, R5747 (1997).
[15] D. C. Ralph, C. T. Black, and M. Tinkham, Phys. Rev. Lett. **74**, 3241 (1995).
[16] R. Desmicht, G. Faini, V. Cros, A. Fert, F. Petroff, and A. Vaures, Appl. Phys. Lett. **72**, 387 (1998).
[17] J. Von Delft and D. Ralph, Phys. Rep. **345**, 61 (2001).
[18] J. Carrey, J.-L. Maurice, F. Petroff, and A. Vaures, Phys. Rev. Lett. **86**, 4600 (2001).
[19] K. Bouzehouane, S. Fusil, M. Bibes, J. Carrey, T. Blon, M. Le Du, P. Seneor, V. Cros, and L. Vila, Nano Lett. **3**, 1599 (2003).
[20] A. E. Hanna and M. Tinkham, Phys. Rev. B **44**, 5919 (1991).
[21] Monte Carlo Single-Electronics Simulator (MOSES), available at http://hana.physics.sunysb.edu/software/MOSES.htm.
[22] R. D. W. F. Brinkman and J. Rowell, J. Appl. Phys. **41**, 1915 (1970).
[23] D. V. Averin and Y. V. Nazarov, Phys. Rev. Lett. **65**, 2446 (1990).
[24] J. Martinek, J. Barnas, S. Maekawa, H. Schoeller, and G. Schon, Phys. Rev. B **66**, 014402 (2002).
[25] I. Weymann, J. Konig, J. Martinek, J. Barnas, and G. Schon, Phys. Rev. B **72**, 115334 (2005).